Heliyon 9 (2023) e17048

Contents lists available at ScienceDirect

Heliyon

journal homepage: www.cell.com/heliyon

# Significantly improved giant dielectric properties and enhanced nonlinear coefficient of $Ni^{2+}$ doped $CaCu_3Ti_4O_{12}$/$CaTiO_3$ composites

Jirata Prachamon [a], Pratumwan Sattapol [a], Narong Chanlek [b], Bundit Putasaeng [c], Nutthakritta Phromviyo [a,d], Viyada Harnchana [a,d], Ekaphan Swatsitang [a,d], Prasit Thongbai [a,d,*]

[a] Giant Dielectric and Computational Design Research Group (GD–CDR), Department of Physics, Faculty of Science, Khon Kaen University, Khon Kaen 40002, Thailand
[b] Synchrotron Light Research Institute (Public Organization), 111 University Avenue, Muang District, Nakhon Ratchasima 30000, Thailand
[c] National Metal and Materials Technology Center, National Science and Technology Development Agency, Thailand Science Park, Pathum Thani 12120, Thailand
[d] Institute of Nanomaterials Research and Innovation for Energy (IN–RIE), Khon Kaen University, Khon Kaen 40002, Thailand

ARTICLE INFO

*Keywords:*
Loss tangent
Ceramic composite
Dielectric properties
Varistor
Impedance spectroscopy

ABSTRACT

$CaCu_{3-x}Ni_xTi_4O_{12}/CaTiO_3$ ceramic composites were fabricated using initial $Ca_2Cu_{2-x}Ni_xTi_4O_{12}$ compositions ($x$ = 0, 0.05, 0.10, and 0.20) to improve the dielectric properties (DPs) of the $CaCu_3Ti_4O_{12}$ ceramics. $CaCu_3Ti_4O_{12}$ and $CaTiO_3$ phases were confirmed. Microstructural analysis and Rietveld refinement showed that the $Ni^{2+}$ dopant might substitute the $Cu^{2+}$ sites of the $CaCu_3Ti_4O_{12}$ structure. The average grain sizes of $CaCu_3Ti_4O_{12}$ (4.1–5.6 μm) and $CaTiO_3$ (1.2–1.4 μm) changed slightly with the $Ni^{2+}$ doping concentration. The best DPs were obtained for the $CaCu_{3-x}Ni_xTi_4O_{12}/CaTiO_3$ with $x = 0.2$. The loss tangent was significantly reduced by an order of magnitude compared to that of the undoped composite, from tanδ~0.161 to ~0.016 at 1 kHz, while the dielectric permittivity slightly decreased from $\varepsilon' \sim 5.7 \times 10^3$ to $\sim 4.0 \times 10^3$. Furthermore, the temperature dependence of $\varepsilon'$ could be improved by doping with $Ni^{2+}$. The improved DPs were caused by the enhanced electrical responses of the internal interfaces, which resulted in enhanced non–Ohmic properties. The largest nonlinear coefficient (α~7.6) was obtained for the $CaCu_{3-x}Ni_xTi_4O_{12}/CaTiO_3$ with $x = 0.05$. Impedance spectroscopy showed that the $CaCu_{3-x}Ni_xTi_4O_{12}/CaTiO_3$ composites consisted of semiconducting and insulating components. The DPs of $CaCu_{3-x}Ni_xTi_4O_{12}/CaTiO_3$ were explained based on the space−charge polarization at the active−interfaces.

## 1. Introduction

The dielectric properties (DPs) of ceramic oxides that exhibit a very large dielectric constant of $\varepsilon' > 10^3$, especially $CaCu_3Ti_4O_{12}$ (CCTO), have been studied owing to their fascinating DPs and promising capacitive materials [1–17]. Unfortunately, the loss tangent

* Corresponding author. Giant Dielectric and Computational Design Research Group (GD–CDR), Department of Physics, Faculty of Science, Khon Kaen University, Khon Kaen 40002, Thailand.
*E-mail address:* pthongbai@kku.ac.th (P. Thongbai).

https://doi.org/10.1016/j.heliyon.2023.e17048
Received 29 January 2023; Received in revised form 3 June 2023; Accepted 6 June 2023
Available online 7 June 2023

(tanδ) of CCTO−based materials remains high. This result is primarily due to the electrically heterogeneous microstructure, in which free charges are present in *n*−type semiconducting grains (*n*−Gs), even though they are enclosed by insulating layers of grain boundaries (*i*−GBs) [2,3]. Thus, engineering *i*−GBs may be the best strategy to improve the DPs of CCTO−based materials.

For CCTO−based oxides, the low−frequency tanδ (Lf−tanδ) value is usually larger than 0.1 [1,4,7–9], which is a large level of dissipation energy over the acceptable value for applications. The large temperature dependence of DPs is another dielectric parameter that is usually difficult to improve. The temperature coefficient $\varepsilon'$ at $10^3$ Hz, i.e., $\Delta\varepsilon'(\%) = [(\varepsilon'_T - \varepsilon'_{RT})]/\varepsilon'_{RT}) \times 100$ (where $\varepsilon'_T$ and $\varepsilon'_{RT}$ are the dielectric permittivities at any temperature (*T*) and room temperature (*RT*), respectively), must be $<\pm$15% in specific temperature ranges of −55 − 125 °C and −55 − 150 °C for the X7R and X8R capacitors [18], respectively. However, when the temperature was increased above 90 °C, $\Delta\varepsilon'(\%)$ increased rapidly to more than 15% [19–23]. The low resistance of the *i*−GBs ($R_{gb}$) is the primary factor for the observed large values of Lf−tanδ and $\Delta\varepsilon'(\%)$. Thus, enhancing $R_{gb}$ to decrease these two parameters is the best way to obtain significantly improved DPs. Generally, CCTO−based oxides exhibit nonlinear current density−electric field (J−E) characteristics. This electrical behavior can be applied to varistor devices [24].

One of the most effective methods to increase $R_{gb}$ is to fabricate CCTO−matrix composites filled with dielectric particles with very low tanδ and high resistivity, such as $CaTiO_3$ (CTO) [25,26]. Notably, CCTO/CTO composites can be fabricated by varying the $Ca^{2+}$:$Cu^{2+}$ ratio in $Ca_{1+x}Cu_{3-x}Ti_4O_{12}$ [5,6,27–32]. The CCTO/CTO exhibited no piezoelectricity. It has been reported that the DPs of CCTO can be remarkably enhanced by doping with $Ni^{2+}$ owing to the increased $R_{gb}$ [33]. Although low tanδ values were obtained for $Ca_2Cu_2Ti_4O_{12}$ (CCTO/CTO) and $CaCu_{2.95}Ni_{0.05}Ti_4O_{12}$ due to the increased $R_{gb}$ values, their $\Delta\varepsilon'(\%)$ values were very large when the temperature was increased to 100 °C [29,32,33]. This is because the total resistance of the *i*−GBs may not be sufficiently large to effectively suppress DC conduction at high temperatures. In this study, the primary approach is to simultaneously use the appropriate dopant substituted into the CCTO matrix composite to obtain reduced tanδ and $\Delta\varepsilon'(\%)$ values. Substitution of $Ni^{2+}$ into the CCTO/CTO composites to further enhance the total $R_{gb}$ value may provide a remarkably reduced Lf−tanδ and obtain temperature stability of the DPs. To the best of our knowledge, the DPs of $Ni^{2+}$−doped CCTO/CTO composites have never been reported. Therefore, the objective of this work is to improve the DPs of CCTO−based oxides using a combination of the ceramic composite method and doping ion approaches.

In this study, $Ni^{2+}$−doped CCTO/CTO composites were fabricated from $Ca_2Cu_{2-x}Ni_xTi_4O_{12}$ compositions. The phase compositions and microstructures were systematically characterized. The DPs and nonlinear J−E properties can be significantly improved, which can be explained by the space−charge polarization at the *i*−GBs.

## 2. Experimental method

$Ca_2Cu_{2-x}Ni_xTi_4O_{12}$ with $x = 0$, 0.05, 0.10, and 0.20 (referred to as the CCTO/CTO, Ni050, Ni100, and Ni200 samples, respectively) were designed to prepare the $Ni^{2+}$−doped CCTO/CTO composites. $CaCO_3$ (99.9%), NiO (99.9%), $TiO_2$ (99.9%), and CuO (99.0%) were mixed in ethanol using a ball−milling method. The details of the preparation steps are provided in our previous paper [34]. First, the starting raw materials were mixed using a ball-milling method in ethanol for 24 h $ZrO_2$ balls with a diameter ~2 mm were used as a grinding media. Second, the $ZrO_2$ balls were separated. Third, the ethanol was evaporated in an oven at 90 °C for 24 h. The powder mixture was then ground carefully. Next, the mixed powders for all compositions were calcined at 900 °C for 15 h to form the phases of CTO and CCTO. Subsequently, the powders were pressed using a uniaxial compressive stress with dimension a 9.5 mm diameter and ~1.8 mm in thickness. Finally, ceramic composite samples were obtained by firing the pellet samples at 1080 °C for 6 h.

The densities of the sintered composites were measured using the Archimedes' method. The characterization techniques of the sintered CCTO/CTO, Ni050, Ni100, and Ni200 samples were field−emission scanning electron microscopy (FE-SEM; HITACHIS SU8030, JAPAN), energy−dispersive X−ray spectroscopy (EDS), X−ray diffraction (XRD, PANalytical), and X−ray photoelectron spectroscopy (XPS). The XRD patterns were measured in a range of $2\theta = 20°$–80° with a step increase of 0.01°/point. Rietveld refinement was performed by analyzing the XRD data using High Score Plus software v3.0e. To reveal the morphology using FE-SEM, the surface of the as−samples were polished and then thermally etched at 1050 °C for 0.5 h. The grain size of any grain was determined from the circumference of the grain. The grain size is defined as the diameter of a circle, where the circumference is equal to that of the grain. The mean grain sizes of the CCTO and CTO phases were averaged. Accordingly, the grain size distribution was calculated. The DPs as functions of temperature (−50 − 210 °C) and frequency (40 − 1 MHz) were tested using A KEYSIGHT E4990A impedance analyzer. Silver paint was used as the electrode for the dielectric and nonlinear electrical measurements. The capacitance–dissipation factor ($C_p$–*D*) mode was selected, where *D* is tanδ. The $\varepsilon'$ value was calculated using the following formula:

$$\varepsilon' = \frac{C_p d}{\varepsilon_0 A}, \tag{1}$$

where *d* and *A* are the sample thickness and the electrode area, respectively. $\varepsilon_0$ is the permittivity of free space ($8.854 \times 10^{-12}$ F/m). The nonlinear electrical characteristics were tested using a high−voltage unit (Keithley Model 247). The nonlinear coefficient ($\alpha$) was calculated using the following formula:

$$\alpha = \frac{log(J_2/J_1)}{log(E_2/E_1)}, \tag{2}$$

where $E_1$ and $E_2$ are the electric fields, at which $J_1 = 1$ and $J_2 = 10$ mA cm$^{-2}$, respectively.

## 3. Results and discussion

The XRD patterns of the CCTO/CTO, Ni050, Ni100, and Ni200 composite samples are shown in Fig. 1(a). The CTO (JCPDS 82−0231) and CCTO (JCPDS 75−2188) phases could be clearly distinguished without the formation of undesirable phases (impurities). The XRD peaks of the CCTO and CTO phases were observed for all samples. However, the peaks at ~30° and ~70° disappeared for the Ni200 sample. The absence of these two peaks is primarily due to the preferential orientation of the (211) plane. The peak at ~45° observed in the Ni200 sample was assigned to the aluminum sample holder for the XRD measurements. The XRD patterns were further characterized using the Rietveld refinement method, as shown in Fig. 1(b)–(e). The data obtained from both phases are summarized in Table 1. The percentages of CCTO and CTO phases for each sample were obtained. The percentage of the CCTO phase in the CCTO/CTO sample was larger than that in the $Ni^{2+}$−doped CCTO/CTO samples. This may be because the atomic mass of Ni is less than that of Cu in the CCTO phase. The XRD patterns of $Ca_2Cu_{2-x}Ni_xTi_4O_{12}$ are similar to those observed in previous works [27–32,35,36]. Considering the molar ratio of $Ca^{2+}$:$Cu^{2+}$ = 2:2, mixed phases of ~66.7 mol% CTO and ~33.3 mol% CCTO occurred. The lattice parameters of both phases changed slightly with variation in $Ni^{2+}$ doping concentration because the ionic radii of $Ni^{2+}$ ($r_4$ = 0.55 Å) and $Cu^{2+}$ ($r_4$ = 0.57 Å) are slightly different [37].

To distinguish the distribution of these two phases in the microstructure, backscattered SEM images of the polished samples are shown in Fig. 2(a)–(d). Lighter and darker grains appeared, which is consistent with Rietveld refinement. According to previously published papers [30–32], the lighter and darker grains were suggested to be the CCTO and CTO phases, respectively. The insets of Fig. 2(a)–(d) show the grain−size distributions of both phases. To further confirm the CTO and CCTO phases, EDS was performed on different grains, as illustrated in Fig. 3. Ca, Ti, and O peaks were observed in the EDS spectra of the lighter and darker grains, whereas Cu was only detected in the lighter grains. Therefore, the lighter and darker grains were confirmed to be the CCTO and CTO phases, respectively. CTO grains with a theoretical volume fraction of ~0.34 were randomly dispersed in the CCTO matrix. The EDS peak of Ni was detected only in lighter grains.

The average grain sizes of the two phases are presented in Table 1. The mean grain sizes of the CCTO and CTO phases in the composite did not change significantly upon $Ni^{2+}$ doping. Generally, abnormal grain growth is observed in CCTO ceramics when the sintering temperature is higher than 1050 °C. Notably, it was not observed in any of the composites even at a sintering temperature of 1080 °C. This observation is described by the pinning effect of inert second−phase particles, such as CTO particles, which can inhibit the GB mobility of the CCTO phase during sintering at a high temperature. The relative densities of more than 93% of all sintered composites are listed in Table 1. The density slightly increased with increasing the $Ni^{2+}$ doping concentration.

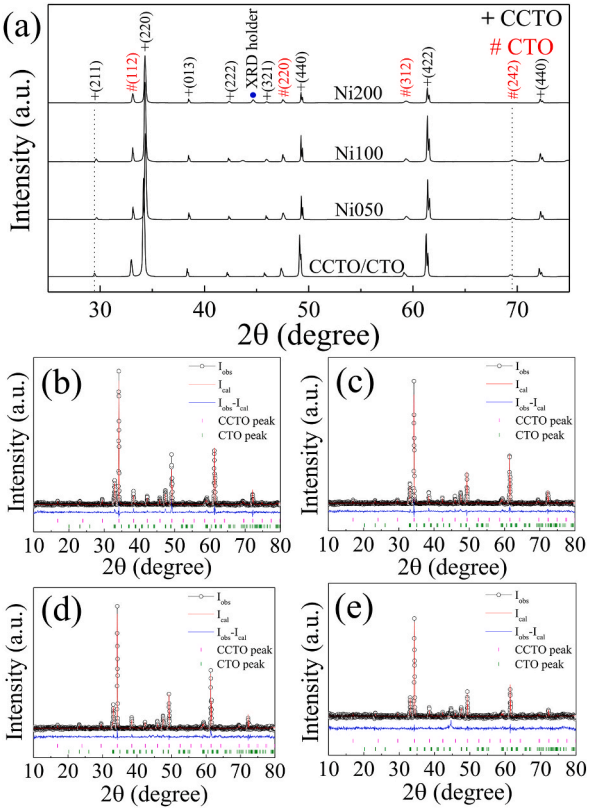


**Fig. 1.** (a) XRD patterns of CCTO/CTO, Ni050, Ni100, and Ni200 composite samples. (b–e) Rietveld profile fit of the patterns obtained for CCTO/CTO, Ni050, Ni100, and Ni200 samples, respectively.

**Table 1**
Lattice parameters, fitting parameters ($R_{exp}$ (%), $R_p$ (%), $R_{wt}$ (%), and GOF), relative density (D), and mean grain sizes ($\overline{G}$) of CCTO and CTO phases for all ceramic composites.

| Sample | CCTO/CTO | Ni050 | Ni100 | Ni200 |
|---|---|---|---|---|
| **CCTO phase** | | | | |
| *a* (Å) | 7.391(3) | 7.394(1) | 7.394(1) | 7.395(2) |
| %CCTO | 74.2(%) | 71.6(%) | 68.5(%) | 71.6(%) |
| **CTO Phase** | | | | |
| *a* (Å) | 5.436(6) | 5.438(9) | 5.438(9) | 5.438(0) |
| *b* (Å) | 7.641(7) | 7.644(1) | 7.643(1) | 7.647(2) |
| *c* (Å) | 5.383(6) | 5.384(8) | 5.382(9) | 5.389(1) |
| %CTO | 27.6(%) | 28.4(%) | 31.5(%) | 28.4(%) |
| **Fitting parameters** | | | | |
| $R_{exp}$ (%) | 11.75 | 13.07 | 13.11 | 11.37 |
| $R_p$ (%) | 8.60 | 9.62 | 9.30 | 6.65 |
| $R_{wt}$ (%) | 9.82 | 8.91 | 9.79 | 7.88 |
| GOF | 1.10 | 1.44 | 1.11 | 1.15 |
| **CCTO/CTO** | | | | |
| D (%) | 93.68% | 93.87% | 97.06% | 97.49% |
| $\overline{G}$: CCTO | 4.1 ± 1.4 | 4.70 ± 2.2 | 5.6 ± 2.1 | 4.7 ± 1.7 |
| $\overline{G}$: CTO | 1.4 ± 1.0 | 1.5 ± 0.9 | 1.3 ± 0.9 | 1.2 ± 0.8 |

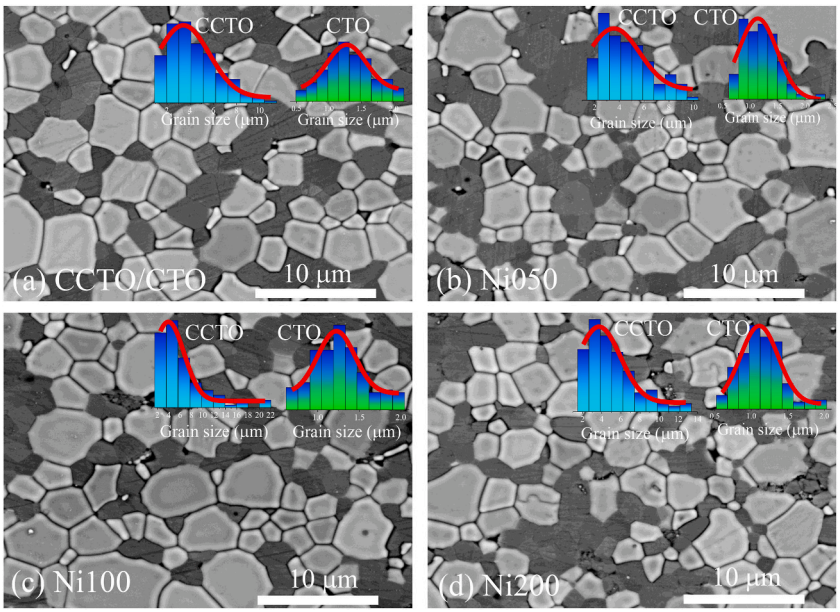


**Fig. 2.** Backscattered SEM images of polished−samples: (a) CCTO/CTO, (b) Ni050, (c) Ni100, and (d) Ni200. Insets of grain size distributions of the CCTO and CTO phases.

The DPs of the composites at 25 °C are shown in Fig. 4 and its inset. The ε′ values were calculated from Eq. (1). The ε′ of the CCTO/CTO decreased with increasing frequency from 40 to $10^4$ Hz, corresponding to a large tanδ value in the low−frequency range. For $Ca_2Cu_{2-x}Ni_xTi_4O_{12}$ with $x = 0.05$ (Ni050), the large frequency−dependence of ε′ was resolved. The ε′ value of Ni050 was almost independent of the frequency over the measured range. The ε′ values of CCTO/CTO and Ni050 were nearly identical in the frequency range of $10^4$–$10^6$ Hz. The dielectric behaviors of Ni100 and Ni200 are similar to that of Ni050. However, their ε′ values were slightly lower than those of Ni050. Nevertheless, the ε′ values of all $Ni^{2+}$−doped CCTO/CTO composites were still very large compared to those of the $BaTiO_3$−based oxides. The dielectric properties at 1 kHz and 25 °C for all the composites were summarized in Table 2. As shown in the inset, the tanδ values of all the composite samples rapidly increased when the frequency was higher than $10^5$ Hz. This behavior is similar to that observed in CCTO ceramics [8,10], which was attributed to dielectric relaxation. Thus, this dielectric behavior is associated with the CCTO phase. It has been demonstrated that the CTO−CTO interface is electrically inactive [19,31]. Thus, the observed dielectric relaxation is likely caused by the dielectric responses of the CTO−CCTO and CCTO−CCTO interfaces. Doping the CCTO/CTO composites with $Ni^{2+}$ can cause a significant decrease in tanδ in the frequency range of 40–$10^5$ Hz. At 1 kHz and 25 °C, the tanδ values of CCTO/CTO, Ni050, Ni100, and Ni200 were 0.161, 0.019, 0.018, and 0.016, respectively. Notably, the tanδ value of CCTO/CTO was significantly reduced by an order of magnitude compared with that of Ni200. Furthermore, the temperature stability

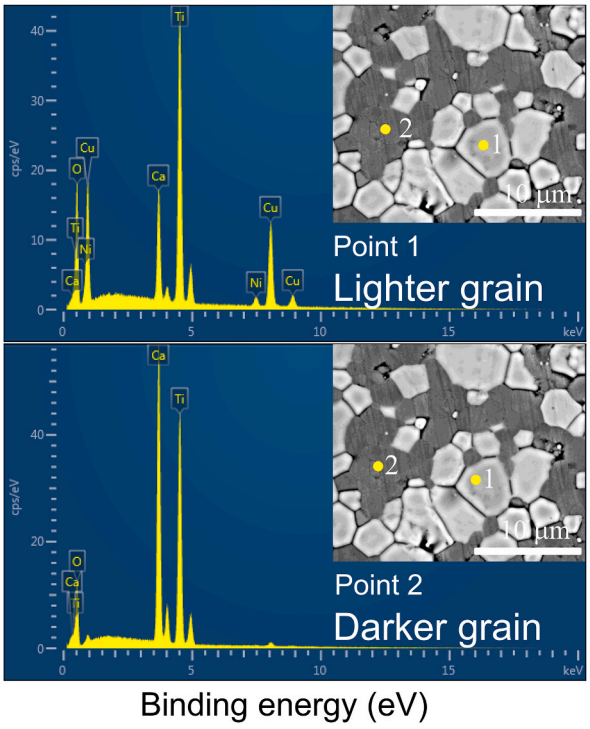


**Fig. 3.** EDS spectra of Ni200 samples detected at points •1 (lighter grains) and •2 (darker grains).

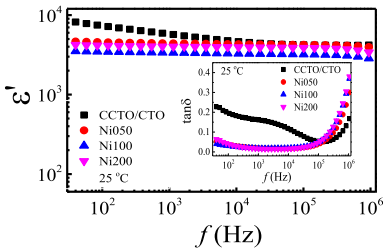


**Fig. 4.** ε′ at 25 °C as a function of frequency for the CCTO/CTO, Ni050, Ni100, and Ni200 composites; the inset shows tanδ for all samples.

**Table 2**
Dielectric properties (ε′ and tanδ) at 1 kHz and ~25 °C and non-linear electrical properties (α and $E_b$) at ~25 °C.

| Sample | Dielectric properties | | Non-linear electrical properties | |
|---|---|---|---|---|
| | ε′ | tanδ | α | $E_b$ (V/cm) |
| **CCTO/CTO** | $5.76 \times 10^3$ | 0.161 | 5.2 | 1196 |
| **Ni050** | $4.41 \times 10^3$ | 0.019 | 7.6 | 744 |
| **Ni100** | $3.36 \times 10^3$ | 0.018 | 6.0 | 1086 |
| **Ni200** | $4.02 \times 10^3$ | 0.016 | 4.9 | 206 |

of ε′ was significantly improved, as shown in Fig. 5. These results indicate that the $Ni^{2+}$ dopant can successfully enhance the DPs of the CCTO/CTO composites.

$Lf - tan\,\delta$ is generally controlled by dc conduction, following the relationship [38] *i.e.*, $Lf - tan\,\delta \approx \sigma_{dc}/\omega\varepsilon_0\varepsilon_s^{'}$ ($\varepsilon_s^{'}$ is a static dielectric constant). For a dielectric oxide with a microstructure consisting of *n*−Gs and *i*−GBs, Lf−tanδ can be suppressed by increasing $R_{gb}$. To describe the significantly decreased $Lf - tan\,\delta$ of the composites due to the $Ni^{2+}$ doping ions, an impedance spectroscopy was used to separate the electrical responses of the *n*−Gs and *i*−GBs in the composites [10,39]. For CCTO−based oxides, the electrical responses of *n*−Gs and *i*−GBs are indicated by a nonzero intercept on the Z′−axis and a large semicircular arc in Z* [10]. Accordingly, $R_{gb}$ can be calculated from the diameter of a large arc. The resistance of the *n*−Gs ($R_g$) was determined by the nonzero intercept. However, if the temperature is sufficiently low and a small semicircular arc appears in the Z* plot, the electrical response in

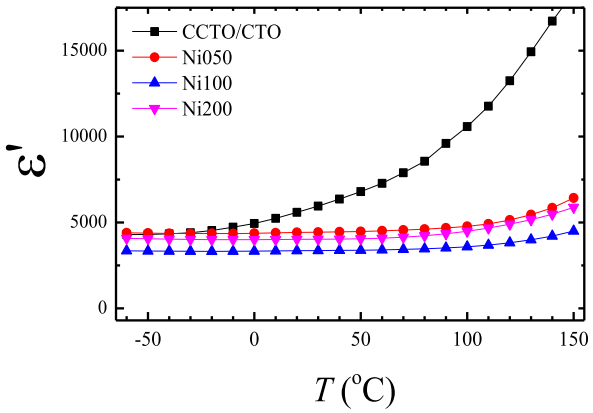


**Fig. 5.** ε′ at 1 kHz as a function of the temperature for the CCTO/CTO, Ni050, Ni100, and Ni200 composites.

*n*−Gs is indicated by a small arc. In this case, the $R_g$ value can be calculated from the diameter of the small arc. Fig. 6 and inset (1) show the impedance complex plane (Z*) plots and nonzero intercepts for all composite samples. Note that a small arc cannot be observed, even at the lowest measured temperature (−60 °C). However, a full large arc of the Z* plots cannot be observed at approximately room temperature and below. Nevertheless, it can be confirmed from the Z* plots that all samples consisted of *n*−Gs and *i*−GBs. Thus, the DPs can be explained based on the space−charge polarization at the internal interfaces, that is, CCTO−CCTO and CCTO−CTO interfaces. Furthermore, the $R_{gb}$ value tended to increase with increasing $Ni^{2+}$ concentration. The significant decrease in Lf−tanδ of the $Ni^{2+}$−doped CCTO/CTO composites was well explained by the remarkable increase in $R_{gb}$, as clearly demonstrated in inset (2) of Fig. 6. It was also observed that $R_g$ of the CCTO/CTO composites increased upon doping with $Ni^{2+}$. This result may be due to the ability of the $Ni^{2+}$ isovalent dopant to fill the oxygen vacancies at the GBs, which is similar to that observed in CCTO ceramics substituted by $Mg^{2+}$ and $Sn^{4+}$ isovalent dopants [40]. The increase in the $R_g$ of the $Ni^{2+}$−doped CCTO/CTO composites was correlated with the decrease in the $Cu^{+}/Cu^{2+}$ ratio, as shown in Fig. S1 (*supplementary information*). According to the theoretical investigations [41], the complex clusters in the CCTO and CTO structures were highly disordered, particularly at the interfaces between these phases. Complex clusters may affect the dielectric or nonlinear electrical properties at the nanoscale level. According to the space−charge polarization at the internal interfaces, the dielectric response is usually dependent on the concentration of free charges ($N_d$) inside n−Gs. The increased $R_g$ values of the $Ni^{2+}$−doped CCTO/CTO composites indicate a decrease in $N_d$ compared to that of the pure CCTO/CTO composite, which is responsible for the observed decrease in ε′ for the $Ni^{2+}$−doped CCTO/CTO composites. For the dielectric response in $x SnO_2$−CCTO/CTO composites [42], doubly−ionized oxygen vacancies ($V_O^{\bullet\bullet}$) caused an increase in the dielectric response at the *i*−GBs [43]. The decrease in the dielectric response of the $Ni^{2+}$−doped CCTO/CTO composites was also due to the suppressed doubly−ionized $V_O^{\bullet\bullet}$ caused by $Ni^{2+}$ doping ions.

Fig. 7 illustrates the nonlinear electrical characteristics of the $Ni^{2+}$−doped CCTO/CTO composites compared with those of the undoped composites. All the composite samples exhibited nonlinear J−E properties. The nonlinear electrical parameters at ~25 °C were listed in Table 2. This was attributed to the formation of a Schottky barrier at the internal interface [43,44]. The breakdown electric field ($E_b$) was calculated at $J = 1$ mA/cm$^2$. The $E_b$ values of CCTO/CTO, Ni050, Ni100, and Ni200 were 1,196, 744, 1086 and 206 V/cm, respectively. It is important to note that $R_{gb}$ and $E_b$ were calculated at different voltage levels. Thus, non−direct relationship exists between these two parameters. The α values were also calculated in the range of J = 1–10 mA/cm$^2$ using Eq. (2) and were found to be 5.2, 7.6, 6.0, and 4.9, respectively. Notably, the α value of the CCTO/CTO composites could be increased by doping with $Ni^{2+}$ at an appropriate concentration. This increased α value indicates a rapid change in the insulator–semiconductor transition, which is suitable for use in varistor devices.

## 4. Conclusions

The DPs of the CCTO/CTO composites, which were prepared using one−step conventional mixed−oxide methods, were successfully improved by doping with $Ni^{2+}$. CCTO and CTO phases were detected in the sintered ceramics with dense microstructures. $Ni^{2+}$ dopant was detected only in the CCTO grains. Doping $Ni^{2+}$ into the $Cu^{2+}$ sites of the CCTO structure caused a slight increase in the average grain size of the CCTO grains, whereas the mean grain size of the CTO grains was nearly independent of $Ni^{2+}$ concentration. CTO grains were randomly dispersed in the CCTO matrix. The tanδ value of the CCTO/CTO composites was significantly reduced by doping with $Ni^{2+}$ compared with that of the undoped composite. Large ε′ values of ~3–5 × 10$^3$ were achieved. Notably. The temperature dependence of ε′ can also be improved significantly. Furthermore, the α value obtained from the J–E characteristics simultaneously increased. Impedance spectroscopy showed that the microstructures of the composites, i.e., *n*−Gs and *i*−GBs, were heterogeneous. The enhanced α and DPs values of the $Ni^{2+}$−doped CCTO/CTO composites were caused by the increased $R_{gb}$. The dielectric behavior was described based on the space−charge polarization at the *i*−GBs.

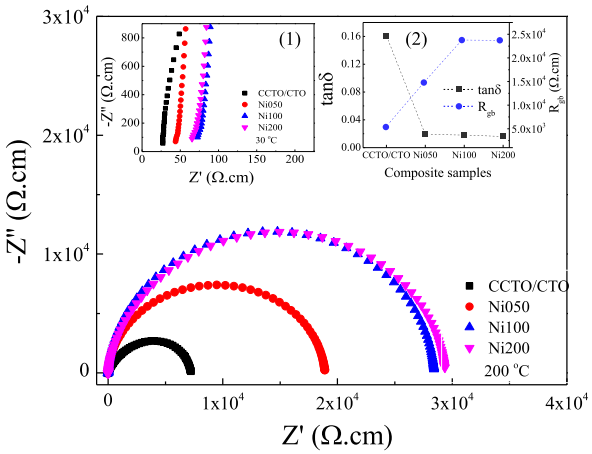


**Fig. 6.** Z* plots of CCTO/CTO, Ni050, Ni100, and Ni200 composites at 200 °C; insets (1) and (2) illustrate a nonzero intercept on the Z′ axis at high frequencies and the relationship between $R_{gb}$ and tanδ at 1 kHz, respectively.

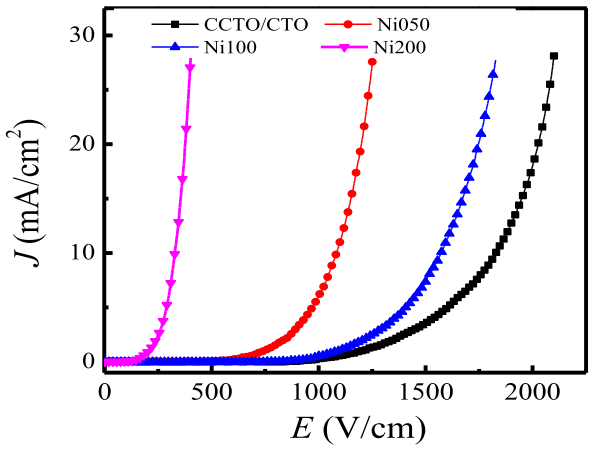


**Fig. 7.** *J–E* characteristics at ~25 °C.

## Author contribution statement

Jirata Prachamon: Conceived and designed the experiments; Performed the experiments; Analyzed and interpreted the data.
Patumwan Sattapol, Bundit Putasaeng: Performed the experiments.
Narong Chanlek: Performed the experiments; Analyzed and interpreted the data.
Nutthakritta Phromviyo, Viyada Harnchana, Ekaphan Swatsitang: Analyzed and interpreted the data.
Prasit Thongbai: Conceived and designed the experiments; Analyzed and interpreted the data; Contributed reagents, materials, analysis tools or data; Wrote the paper.

## Data availability statement

Data will be made available on request.

## Declaration of Competing Interest

The authors declare that they have no known competing financial interests or personal relationships that could have appeared to influence the work reported in this paper

## Acknowledgments

This project was funded by the National Research Council of Thailand (NRCT): (N41A640084). This research received funding

support from Research and Graduate Studies of Khon Kaen University. J. Prachamon would like to thank the Institute of Nanomaterials Research and Innovation for Energy (IN–RIE), Khon Kaen University, for Ph.D. scholarship.

## Appendix A. Supplementary data

Supplementary data to this article can be found online at https://doi.org/10.1016/j.heliyon.2023.e17048.

## References

[1] M.A. Subramanian, D. Li, N. Duan, B.A. Reisner, A.W. Sleight, High dielectric constant in $ACu_3Ti_4O_{12}$ and $ACu_3Ti_3FeO_{12}$ phases, J. Solid State Chem. 151 (2000) 323–325, https://doi.org/10.1006/jssc.2000.8703.
[2] D.C. Sinclair, T.B. Adams, F.D. Morrison, A.R. West, $CaCu_3Ti_4O_{12}$: one-step internal barrier layer capacitor, Appl. Phys. Lett. 80 (2002) 2153, https://doi.org/10.1063/1.1463211.
[3] S.-Y. Chung, I.-D. Kim, S.-J.L. Kang, Strong nonlinear current–voltage behaviour in perovskite-derivative calcium copper titanate, Nat. Mater. 3 (2004) 774–778, https://doi.org/10.1038/nmat1238.
[4] E.A. Patterson, S. Kwon, C.-C. Huang, D.P. Cann, Effects of $ZrO_2$ additions on the dielectric properties of $CaCu_3Ti_4O_{12}$, Appl. Phys. Lett. 87 (2005), 182911, https://doi.org/10.1063/1.2126142.
[5] W. Kobayashi, I. Terasaki, $CaCu_3Ti_4O_{12}/CaTiO_3$ composite dielectrics: Ba/Pb-free dielectric ceramics with high dielectric constants, Appl. Phys. Lett. 87 (2005), 032902, https://doi.org/10.1063/1.1997278.
[6] M.A. Ramírez, P.R. Bueno, J.A. Varela, E. Longo, Non-Ohmic and dielectric properties of a $Ca_2Cu_2Ti_4O_{12}$ polycrystalline system, Appl. Phys. Lett. 89 (2006), 212102, https://doi.org/10.1063/1.2393122.
[7] M. Li, G. Cai, D.F. Zhang, W.Y. Wang, W.J. Wang, X.L. Chen, Enhanced dielectric responses in Mg-doped $CaCu_3Ti_4O_{12}$, J. Appl. Phys. 104 (2008), 074107, https://doi.org/10.1063/1.2989124.
[8] L. Ni, X.M. Chen, Enhanced giant dielectric response in Mg-substituted $CaCu_3Ti_4O_{12}$ ceramics, Solid State Commun. 149 (2009) 379–383, https://doi.org/10.1016/j.ssc.2008.12.016.
[9] L. Ni, X.M. Chen, Enhancement of giant dielectric response in $CaCu_3Ti_4O_{12}$ ceramics by Zn substitution, J. Am. Ceram. Soc. 93 (2010) 184–189, https://doi.org/10.1111/j.1551-2916.2009.03384.x.
[10] R. Schmidt, M.C. Stennett, N.C. Hyatt, J. Pokorny, J. Prado-Gonjal, M. Li, D.C. Sinclair, Effects of sintering temperature on the internal barrier layer capacitor (IBLC) structure in $CaCu_3Ti_4O_{12}$ (CCTO) ceramics, J. Eur. Ceram. Soc. 32 (2012) 3313–3323, https://doi.org/10.1016/j.jeurceramsoc.2012.03.040.
[11] W. Li, L. Tang, F. Xue, Z. Xin, Z. Luo, G. Du, Large reduction of dielectric losses of $CaCu_3Ti_4O_{12}$ ceramics via air quenching, Ceram. Int. 43 (2017) 6618–6621, https://doi.org/10.1016/j.ceramint.2017.02.029.
[12] G. Du, F. Wei, W. Li, N. Chen, Co-doping effects of A-site $Y^{3+}$ and B-site $Al^{3+}$ on the microstructures and dielectric properties of $CaCu_3Ti_4O_{12}$ ceramics, J. Eur. Ceram. Soc. 37 (2017) 4653–4659, https://doi.org/10.1016/j.jeurceramsoc.2017.06.046.
[13] Z. Peng, X. Zhou, J. Wang, J. Zhu, P. Liang, X. Chao, Z. Yang, Origin of colossal permittivity and low dielectric loss in $Na_{1/3}Cd_{1/3}Y_{1/3}Cu_3Ti_4O_{12}$ ceramics, Ceram. Int. 46 (2020) 11154–11159, https://doi.org/10.1016/j.ceramint.2020.01.136.
[14] Z. Peng, J. Wang, X. Zhou, J. Zhu, X. Lei, P. Liang, X. Chao, Z. Yang, Grain engineering inducing high energy storage in $CdCu_3Ti_4O_{12}$ ceramics, Ceram. Int. 46 (2020) 14425–14430, https://doi.org/10.1016/j.ceramint.2020.02.239.
[15] Z. Peng, X. Wang, S. Xu, F. Zhang, J. Wang, J. Wang, D. Wu, P. Liang, L. Wei, X. Chao, Z. Yang, Improved grain boundary resistance inducing decreased dielectric loss and colossal permittivity in $Y_{2/3}Cu_3Ti_4O_{12}$ ceramics, Mater. Chem. Phys. (2022), 125874, https://doi.org/10.1016/j.matchemphys.2022.125874.
[16] Z. Peng, J. Wang, X. Lei, J. Zhu, S. Xu, P. Liang, L. Wei, D. Wu, J. Wang, X. Chao, Z. Yang, Colossal dielectric response in $CdAl_xCu_{3-x}Ti_4O_{12}$ perovskite ceramics, Mater. Chem. Phys. 258 (2021), 123940, https://doi.org/10.1016/j.matchemphys.2020.123940.
[17] Q. Hu, J. Tang, Y. Teng, X. Zhao, T. Arslanov, R. Ahuja, Preparation and dielectric properties of La doped NBCCTO ceramics, J. Electroceram. 48 (2022) 117–126, https://doi.org/10.1007/s10832-022-00280-z.
[18] M. Pan, C.A. Randall, A brief introduction to ceramic capacitors, IEEE Electr. Insul. Mag. 26 (2010) 44–50, https://doi.org/10.1109/MEI.2010.5482787.
[19] M. Li, D.F. Zhang, W.Y. Wang, G. Wang, X.L. Chen, The effects of grain boundary response and electrode contact response on the dielectric properties of $CaCu_3Ti_4O_{12}$, J. Phys. D Appl. Phys. 43 (2010), 295405, https://doi.org/10.1088/0022-3727/43/29/295405.
[20] Z. Yang, L. Zhang, X. Chao, L. Xiong, J. Liu, High permittivity and low dielectric loss of the $Ca_{1-x}Sr_xCu_3Ti_4O_{12}$ ceramics, J. Alloys Compd. 509 (2011) 8716–8719, https://doi.org/10.1016/j.jallcom.2011.06.039.
[21] P. Liang, Z. Yang, X. Chao, Z. Liu, X.M. Chen, Giant dielectric constant and good temperature stability in $Y_{2/3}Cu_3Ti_4O_{12}$ ceramics, J. Am. Ceram. Soc. 95 (2012) 2218–2225, https://doi.org/10.1111/j.1551-2916.2012.05152.x.
[22] P. Liang, X. Chao, F. Wang, Z. Liu, Z. Yang, The lowered dielectric loss and grain-boundary effects in La-doped $Y_{2/3}Cu_3Ti_4O_{12}$ ceramics, J. Am. Ceram. Soc. 96 (2013) 3883–3890, https://doi.org/10.1111/jace.12644.
[23] Y. Li, P. Liang, X. Chao, Z. Yang, Preparation of $CaCu_3Ti_4O_{12}$ ceramics with low dielectric loss and giant dielectric constant by the sol–gel technique, Ceram. Int. 39 (2013) 7879–7889, https://doi.org/10.1016/j.ceramint.2013.03.049.
[24] L.J. Brillson, Y. Lu, ZnO Schottky barriers and Ohmic contacts, J. Appl. Phys. 109 (2011), 121301, https://doi.org/10.1063/1.3581173.
[25] W. Kobayashi, I. Terasaki, $CaCu_3Ti_4O_{12}/CaTiO_3$ composite dielectrics: Ba/Pb-free dielectric ceramics with high dielectric constants, Appl. Phys. Lett. 87 (2005), 032902, https://doi.org/10.1063/1.1997278.
[26] M. Maleki Shahraki, H. Daeijavad, A.H. Emami, M. Abdollahi, A. Karimi, An engineering design based on nano/micro-sized composite for $CaTiO_3/CaCu_3Ti_4O_{12}$ materials and its dielectric and non-Ohmic properties, Ceram. Int. 45 (2019) 21676–21683, https://doi.org/10.1016/j.ceramint.2019.07.166.
[27] L. Ramajo, R. Parra, J.A. Varela, M.M. Reboredo, M.A. Ramírez, M.S. Castro, Influence of vanadium on electrical and microstructural properties of $CaCu_3Ti_4O_{12}/CaTiO_3$, J. Alloys Compd. 497 (2010) 349–353, https://doi.org/10.1016/j.jallcom.2010.03.064.
[28] T. Li, K. Fang, J. Hao, Y. Xue, Z. Chen, The effect of Ca-rich on the electric properties of $Ca_{1+x}Cu_{3-x}Ti_4O_{12}$ polycrystalline system, Mater. Sci. Eng. B 176 (2011) 171–176, https://doi.org/10.1016/j.mseb.2010.10.010.
[29] P. Thongbai, B. Putasaeng, T. Yamwong, S. Maensiri, Improved dielectric and non-ohmic properties of $Ca_2Cu_2Ti_4O_{12}$ ceramics prepared by a polymer pyrolysis method, J. Alloys Compd. 509 (2011) 7416–7420, https://doi.org/10.1016/j.jallcom.2011.04.052.
[30] M.A. Ramírez, P.R. Bueno, E. Longo, J.A. Varela, Conventional and microwave sintering of $CaCu_3Ti_4O_{12}/CaTiO_3$ ceramic composites: non-ohmic and dielectric properties, J. Phys. D Appl. Phys. 41 (2008), 152004, https://doi.org/10.1088/0022-3727/41/15/152004.
[31] M.A. Ramírez, P.R. Bueno, R. Tararam, A.A. Cavalheiro, E. Longo, J.A. Varela, Evaluation of the effect of the stoichiometric ratio of Ca/Cu on the electrical and microstructural properties of the $CaCu_3Ti_4O_{12}$ polycrystalline system, J. Phys. D Appl. Phys. 42 (2009), 185503, https://doi.org/10.1088/0022-3727/42/18/185503.
[32] J. Jumpatam, P. Thongbai, B. Kongsook, T. Yamwong, S. Maensiri, High permittivity, low dielectric loss, and high electrostatic potential barrier in $Ca_2Cu_2Ti_4O_{12}$ ceramics, Mater. Lett. 76 (2012) 40–42, https://doi.org/10.1016/j.matlet.2012.02.054.
[33] L. Sun, R. Zhang, Z. Wang, E. Cao, Y. Zhang, L. Ju, Microstructure, dielectric properties and impedance spectroscopy of Ni doped $CaCu_3Ti_4O_{12}$ ceramics, RSC Adv. 6 (2016) 55984–55989, https://doi.org/10.1039/C6RA07726A.

[34] J. Prachamon, J. Boonlakhorn, N. Chanlek, N. Phromviyo, V. Harnchana, P. Srepusharawoot, E. Swatsitang, P. Thongbai, Enhanced dielectric response and non-Ohmic properties of Ge-doped $CaTiO_3/CaCu_3Ti_4O_{12}$, J. Asian Ceram. Societies 10 (2022) 473–481, https://doi.org/10.1080/21870764.2022.2072569.
[35] B. Cheng, Y.-H. Lin, H. Yang, J. Lan, C.-W. Nan, X. Xiao, J. He, High dielectric permittivity behavior in Cu-doped $CaTiO_3$, J. Am. Ceram. Soc. 92 (2009) 2776–2779, https://doi.org/10.1111/j.1551-2916.2009.03254.x.
[36] L.H. Oliveira, E.C. Paris, W. Avansi, M.A. Ramirez, V.R. Mastelaro, E. Longo, J.A. Varela, X.M. Chen, Correlation between photoluminescence and structural defects in $Ca_{1+x}Cu_{3-x}Ti_4O_{12}$ systems, J. Am. Ceram. Soc. 96 (2013) 209–217, https://doi.org/10.1111/jace.12020.
[37] R.D. Shannon, Revised effective ionic radii and systematic Studies of interatomie distances in halides and chaleogenides, Acta Crystallogr. A32 (1976) 751–767, https://doi.org/10.1016/j.ceramint.2013.08.123.
[38] J. Wu, C.-W. Nan, Y. Lin, Y. Deng, Giant dielectric permittivity observed in Li and Ti doped NiO, Phys. Rev. Lett. 89 (2002), 217601, https://doi.org/10.1103/PhysRevLett.89.217601.
[39] T.B. Adams, D.C. Sinclair, A.R. West, Influence of processing conditions on the electrical properties of $CaCu_3Ti_4O_{12}$ ceramics, J. Am. Ceram. Soc. 89 (2006) 3129–3135, https://doi.org/10.1111/j.1551-2916.2006.01184.x.
[40] J. Boonlakhorn, B. Putasaeng, P. Kidkhunthod, J. Manyam, S. Krongsuk, P. Srepusharawoot, P. Thongbai, First-principles calculations and experimental study of enhanced nonlinear and dielectric properties of $Sn^{4+}$-doped $CaCu_{2.95}Mg_{0.05}Ti_4O_{12}$ ceramics, J. Eur. Ceram. Soc. 41 (2021) 5176–5183, https://doi.org/10.1016/j.jeurceramsoc.2021.04.017.
[41] L.H. Oliveira, M.A. Ramírez, M.A. Ponce, L.A. Ramajo, A.R. Albuquerque, J.R. Sambrano, E. Longo, M.S. Castro, F.A. La Porta, Optical and gas-sensing properties, and electronic structure of the mixed-phase $CaCu_3Ti_4O_{12}/CaTiO_3$ composites, Mater. Res. Bull. 93 (2017) 47–55, https://doi.org/10.1016/j.materresbull.2017.04.037.
[42] G. Cotrim, J.A. Cortés, H. Moreno, S.M. Freitas, M.V.S. Rezende, L.R.O. Hein, M.A. Ramírez, Tunable capacitor-varistor response of $CaCu_3Ti_4O_{12}/CaTiO_3$ ceramic composites with $SnO_2$ addition, Mater. Char. 170 (2020), 110699, https://doi.org/10.1016/j.matchar.2020.110699.
[43] J.A. Cortés, G. Cotrim, S. Orrego, A.Z. Simões, M.A. Ramírez, Dielectric and non-ohmic properties of $Ca_2Cu_2Ti_{4-x}Sn_xO_{12}$ ($0.0 \leq x \leq 4.0$) multiphasic ceramic composites, J. Alloys Compd. 735 (2018) 140–149, https://doi.org/10.1016/j.jallcom.2017.11.089.
[44] T. Adams, D. Sinclair, A. West, Characterization of grain boundary impedances in fine- and coarse-grained $CaCu_3Ti_4O_{12}$ ceramics, Phys. Rev. B 73 (2006), 094124, https://doi.org/10.1103/PhysRevB.73.094124.